Asymmetric Bidirectional Capacitive Power Transfer Method With Push–Pull Full-Bridge Hybrid Topology

Xin Dai, *Member, IEEE*, Min Sun, Pengqi Deng, Rui Wang, and Yugang Su, *Member, IEEE*

***Abstract*—Bidirectional capacitive power transfer technology makes it possible for energy sharing among multiple electronic devices. This article proposes an asymmetrical bidirectional power conversion topology to satisfy different input and output characteristics' requirements and increase load variation tolerance. A π–T (*CLC–LCL*) resonant topology is designed for this bidirectional conversion mode with constant output voltage characteristics in both directions. A hybrid power flow regulation strategy is proposed by integrating multiple zero-voltage switching soft-switching operating points switching and phase-shifted mode. This method overcomes the problem of mixing two different type topologies (push–pull and full bridge) with two different power regulation modes (switch soft-switching operating points and phase shift), which provide a way to make two different chargers compatible. Simulation and experimental results verified the proposed method.**

***Index Terms*—Asymmetric, bidirectional capacitive power transfer system, dynamic switching, phase shifted, soft-switching operating points, steady-state operation.**

I. Introduction

With the rapid development of mobile electronic products, consumers expect that their mobile devices can easily share energy wirelessly for the environments without an available power grid supply. Therefore, bidirectional wireless power transfer (BWPT) systems gradually show their unique advantages. This wireless interface is bidirectional to exchange energy for energy balancing to optimize the function of "need" charging between different power rating devices. It is advantageous for the devices to share energy to the best effect and provides safe and flexible operations even in very harsh environments [1].

In the past, the dual active bridge (DAB) converter utilized the leakage inductance of the transformer as the main energy transfer element to realize the bidirectional power flow [2]. The full-bridge bidirectional inductive power transfer (BIPT) system is similar to the DAB converter, which changes the transformer into a wireless power transmission device. BIPT system has many applications, mainly including portable phones, robot arms, and electric vehicles (EVs) [3]–[5], and research articles mainly in investigating the function realization of bidirectional power flow, model establishing of power flow, the synchronous signal controlling technology, control strategy optimizing technology [5]–[7], etc. However, the coupling structure is normally bulky and costly by using the inductive power transfer (IPT) method, which is not easy to be embedded in compact devices. Compared with the IPT systems, capacitive power transfer (CPT) technology utilizes electric field coupling for wireless power transfer. It has some special advantages, including encountering metal objects without generating significant power losses, small eddy current loss, light, and low cost of coupling structure [8]–[11]. Therefore, the CPT system has attracted lots of experts to research widely on the applications of EVs, rotating mechanisms, mobile robots, biomedical implants, portable electronic devices, and has made some achievements [12]–[16].

At present, research on CPT technology is almost limited to unidirectional transmission, and various symmetrical circuit topologies or compensation strategies are proposed. Zhang *et al.* [17] introduce four plates symmetrical CPT system with *LCL* compensation topology. A dual *LCLC*-compensated symmetrical CPT system is proposed in [18]; the system is developed for EVs. Lu *et al.* [19] propose a symmetrical *LC* resonant network CPT system in which the capacitor is connected in parallel with the plates to reduce the compensation inductor and increases the transmission distance under the same transmission performance. These symmetrical CPT systems proposed in the literature are designed for unidirectional power flow transmission.

The bidirectional capacitive power transmission (BCPT) concept is emerging in recent papers. Yang *et al.* [20] proposed a BCPT system with dual symmetric *LCLC* topology, which is developed for autonomous underwater vehicle (AUV) applications. Bidirectional power flow transmission is realized by leading and lagging 90° by the primary and receiver converters, respectively. However, it did not mention the power flow regulation method.

It can be concluded that previous research articles on the BCPT system utilize the traditional symmetric topology in BWPT systems. However, the traditional symmetrical converter and topological structure used in the BWPT system may limit the performance optimization and expansion in some aspects; it mainly includes the following.

1) Low system voltage gain problem. The symmetrical topology has two symmetrical full-bridge converters. Its advantage is a large power rating, whereas its disadvantage is the system voltage transfer gain that is limited. To achieve

Manuscript received 31 December 2021; revised 31 March 2022; accepted 10 May 2022. Date of publication 19 May 2022; date of current version 26 July 2022. This work was supported by the National Natural Science Foundations of China under Grant 51977015. Recommended for publication by Associate Editor O. Lucia. *(Corresponding author: Xin Dai.)*

The authors are with the School of Automation, Chongqing University, Chongqing 400044, China (e-mail: toybear@vip.sina.com; 1124755093@qq.com; 357619947@qq.com; 573328642@qq.com; su7558@qq.com).

Color versions of one or more figures in this article are available at https://doi.org/10.1109/TPEL.2022.3175477.

Digital Object Identifier 10.1109/TPEL.2022.3175477

enough large output voltage, an auxiliary dc–dc converter is needed, which will increase the volume and cost of the whole system.

2) Topology limitation. As the BWPT system is concerned, symmetrical topology is mostly a selected topology structure. However, it has a strong limitation that makes system characteristic very tough and inflexible. On the contrary, asymmetrical topology structures will expand more adaptive current-fed resonant topologies to achieve custom performance requirement.
3) Lower loss consideration. The main characteristic of the CPT system is the high operating frequency. The full-bridge converter topology with the traditional phase-shifting voltage regulation method will bring some difficulties in switching components when compared with operated at soft-switching frequencies by the push–pull converter.
4) Load variation tolerance problem. Due to the CPT system being sensitive to the system parameters under high-frequency conditions, a small difference with load variation will cause a large disturbance on system output or result in large inherent frequency drifting. So, it is better to design a constant output voltage topology for the bidirectional power transmission system.

To design an asymmetrical topology for the BWPT system, we should consider completely different input characteristics and output power regulation modes with voltage-fed and current-fed converters. Furthermore, forward and reverse resonant circuit element parameters should be carefully balanced to reach approximate constant output voltage requirements. Besides, it is necessary to expand the type of topologies to make them adaptive to present CPT applications. Therefore, the article performs an asymmetrical topology by two types of the converter to realize the system bidirectional transmission.

This article proposes an asymmetrical π–T topology BCPT system by using the push–pull and full-bridge converter, which is suitable for the applications of constant voltage systems. The rest of this article is organized as follows. Section II introduces the proposed BCPT system and explains the steady-state operation of forward and reverse power transmissions. This section also discusses the characteristics of the system topology. Section III shows the power regulation method of the bidirectional power flow by switching zero-voltage switching (ZVS) soft-switching operation points during forward power transmission direction and phase-shifted control during reverse power transmission direction. Section IV provides the performance analysis of the proposed system. The implementation of bidirectional power flow is verified by the experimental results for both power transmission directions in Section V. The discussion is drawn in Section VI. Finally, Section VII concludes this article.

II. Proposed BCPT System

To enhance the voltage gain and load variation tolerance performance, an asymmetrical bidirectional push–pull full-bridge converter and π–T resonance network topology BCPT system is proposed, as shown in Fig. 1. The proposed system includes

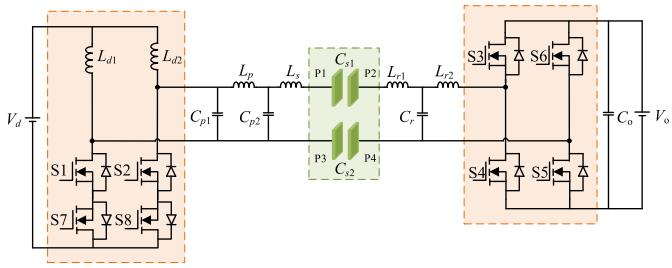

Fig. 1. Circuit topology of the push–pull full-bridge π–T compensated BCPT system.

a current-fed push–pull converter, a full-bridge converter, dc inductors L_{d1} and L_{d2}, and dc filter capacitor C_o. The π-*CLC* (C_{p1}–L_p–C_{p2}) and the T-*LCL* (L_{r1}–C_r–L_{r2}) hybrid resonant topologies, which are suitable for the asymmetrical current-fed push–pull and voltage-fed full-bridge resonant converter, are proposed in the proposed BCPT system. Considering that each side may work as a source or a load, V_d and V_o are expressed as forward and reverse dc input voltages, respectively. Power flows through the coupling capacitances with four plates, which can be classified by transmitter plate pair and receiver pair. C_{s1} and C_{s2} are the two pairs of equivalent capacitances of the coupling plates. The inductor L_s is placed in series with the equivalent capacitance C_s to compensate for the reactive power circulation in the resonant circuit, where $C_s = C_{s1}C_{s2}/(C_{s1}+C_{s2})$.

Since the asymmetrical topology is adopted, the system operation principle should be given for forward and reverse transmissions, respectively. To illustrate the operation principle of the push–pull and full-bridge converter, a steady-state analysis of each switching interval is given. *SD*1–*SD*8 represent the body diodes of the switches *S*1–*S*8. The voltage and current of the switches are v_{S1}–v_{S8} and i_{S1}–i_{S8}, and which of the body diodes are v_{SD1}–v_{SD8} and i_{SD1}–i_{SD8}, respectively. Besides, v_d and i_d are the dc input voltage and current of the push–pull converter, i_{d1} and i_{d2} are the currents through inductors L_{d1} and L_{d2}, v_o is the voltage across the capacitor C_o, and v_p, v_r and i_p, i_r represent the voltages and currents of the converters, respectively.

A. Steady-State Operation of Forward Power Transmission

During forward power transmission direction, the current-fed push–pull converter acts as an inverter and the full-bridge converter acts as a rectifier. The converter leg switches *S*1 and *S*2 are operated at a fixed duty cycle, while *S*3–*S*8 are turned OFF. The steady-state analysis, operating waveforms, and equivalent circuits of the converters for forward power transmission operation are discussed, as shown in Fig. 2.

Interval I ($t_1 \le t < t_2$):

Considering that at instant t_1, switch *S*1 is turned OFF and *S*2 is turned ON, while *S*7 and *S*8 are turned OFF. It is shown in Figs. 2 and 3(a) that dc-link current i_d passed through switches *S*2 and *S*8 completely. From this instant, the output voltage of the push–pull converter crosses zero and changes from positive to negative, and the switches *S*1 and *S*7 get a positive voltage. The current polarity passing through L_{r2} changes from positive

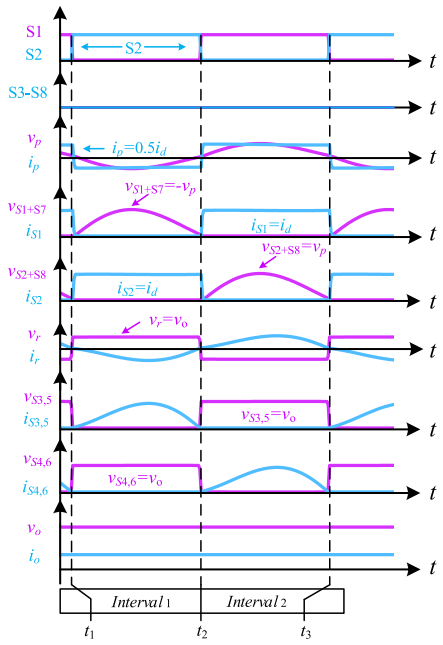

Fig. 2. Steady-state operation waveforms of the converter during forward power transmission.

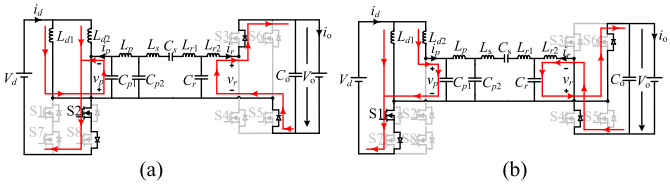

Fig. 3. Equivalent circuits for different switching intervals during forward power transmission. (a) t_1–t_2. (b) t_2–t_3.

to negative, body diodes *SD*4, *SD*6 turn-OFF at zero current, and zero reverse recovery of *SD*3, *SD*5 is achieved.

Interval II ($t_2 \le t < t_3$):

At instant t_2, push–pull converter voltage changes polarity and switch *S*1 starts conducting, as shown in Fig. 3(b). During this interval, a positive voltage with the same magnitude as v_p appears in the switches *S*2 and *S*8. The body diodes *SD*3 and *SD*5 are turned OFF by the presence of reverse current i_r, whereas *SD*4 and *SD*6 conduct.

B. Steady-State Operation of Reverse Power Transmission

Opposite to the forward power transmission operation, during reverse power transmission direction, the full-bridge converter acts as a voltage-fed inverter and the push–pull converter acts as a current-doubled rectifier. The current-fed push–pull converter switches *S*1 and *S*2 are turned OFF and body diodes *SD*1 and *SD*2 act as rectifier diodes, while *S*7 and *S*8 are turned ON. Fig. 4 shows the reverse power transmission waveforms during steady-state operation, and Fig. 5 shows an equivalent circuit diagram of each switching interval.

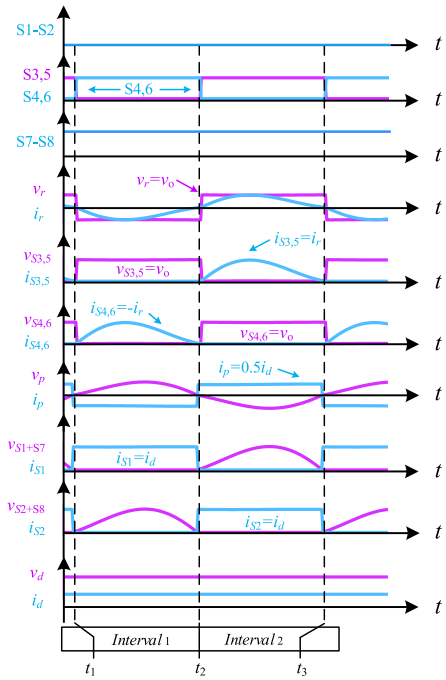

Fig. 4. Steady-state operation waveforms of the converter during reverse transmission.

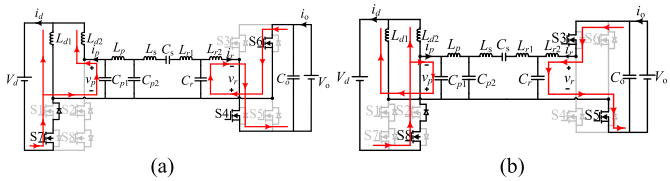

Fig. 5. Equivalent circuits for different switching intervals during reverse power transmission. (a) t_1–t_2. (b) t_2–t_3.

Interval I ($t_1 \le t < t_2$):

In this interval, *S*4, *S*6 are turned ON and *S*3, *S*5 are turned OFF. A negative voltage of v_r appears at the output of the full-bridge converter and due to the presence of T-*LCL* resonant tank, a high excitation voltage crosses through the coupling plates, as shown in Figs. 4 and 5(a). The ac-side voltage of pull–push converter side becomes positive and the body diode *SD*2 is reversely biased, whereas body diode *SD*1 is turned ON and becomes forward biased, which flows through the current i_d.

Interval II ($t_2 \le t < t_3$):

At instant t_2, switches *S*3, *S*5 are turned ON and *S*4, *S*6 are turned OFF. The polarity of the full-bridge converter voltage changes to positive. The switch *S*3 is passed through current i_r, and the body diode *SD*2 is in the forward direction, as shown in Fig. 5(b). In this interval, the inductance current i_d passes through the π-*CLC* resonant network of the system, and the body diode *SD*2 conducts because the magnitude of voltage v_p is negative.

Based on the steady-state analysis of the BCPT system, the relations of the voltage and current at all switching intervals

TABLE I
VOLTAGE AND CURRENT EXPRESSIONS OF THE CONVERTER SIDE COMPONENTS DURING FORWARD AND REVERSE DIRECTIONS

	Forward direction	Reverse direction
Interval I	$i_{S2}=i_{d1}+i_{d2}$	$v_{S3,5}=v_o$
	$L_{d2}\frac{di_{d2}}{dt}=v_d$	$i_{S4,6}=-i_r$
	$L_{d1}\frac{di_{d1}}{dt}=v_d+v_p$	$C_o\frac{dv_o}{dt}=i_o-i_r$
	$v_{S4,6}=v_o$	$v_{S2+S8}=v_p$
	$i_{S3,5}=-i_r$	$L_{d2}\frac{di_{d2}}{dt}=v_d-v_p$
	$C_o\frac{dv_o}{dt}=-i_o+i_r$	$L_{d1}\frac{di_{d1}}{dt}=v_d$
Interval II	$i_{S1}=i_{d1}+i_{d2}$	$v_{S4,6}=v_o$
	$L_{d1}\frac{di_{d1}}{dt}=v_d$	$i_{S3,5}=i_r$
	$L_{d2}\frac{di_{d2}}{dt}=v_d-v_p$	$C_o\frac{dv_o}{dt}=i_o-i_r$
	$v_{S3,5}=v_o$	$v_{S1+S7}=-v_p$
	$i_{S4,6}=i_r$	$L_{d1}\frac{di_{d1}}{dt}=v_d+v_p$
	$C_o\frac{dv_o}{dt}=-i_o+i_r$	$L_{d2}\frac{di_{d2}}{dt}=v_d$

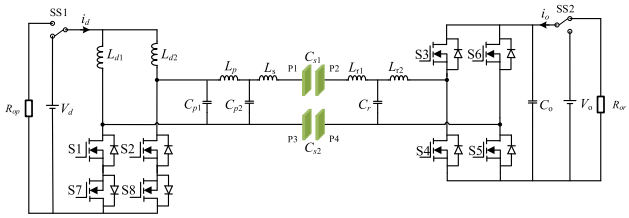

Fig. 6. Circuit topology with power source and load switching of the proposed BCPT system.

during forward and reverse power transmission directions can be concluded in Table I.

C. Dynamic Switching Process

The dual load resistance and dc power source of the proposed BCPT system connected in parallel are shown in Fig. 6. The ON/OFF of the two branches is controlled via relay-operated switches.

Switching pulses with all system switches during both power directions are shown in Fig. 7. The orange line represents the switching switches *SS*1 and *SS*2 of the power source and load resistance in parallel on the dual converter sides. When *SS*1/*SS*2 = 1, which represents the power source branch is "ON"; *SS*1/*SS*2 = 0, which means the resistance branch is "ON." The blue line represents the switches *S*1–*S*8 of the converters. The red line represents the dc current i_d and i_o.

When $t<t_1$, the system operates in the forward power transmission, the converter of the full bridge acts as a rectifier, and the load resistance R_{or} receives energy. The power source branch V_d with the push–pull converter is "ON," while the load R_{op} is

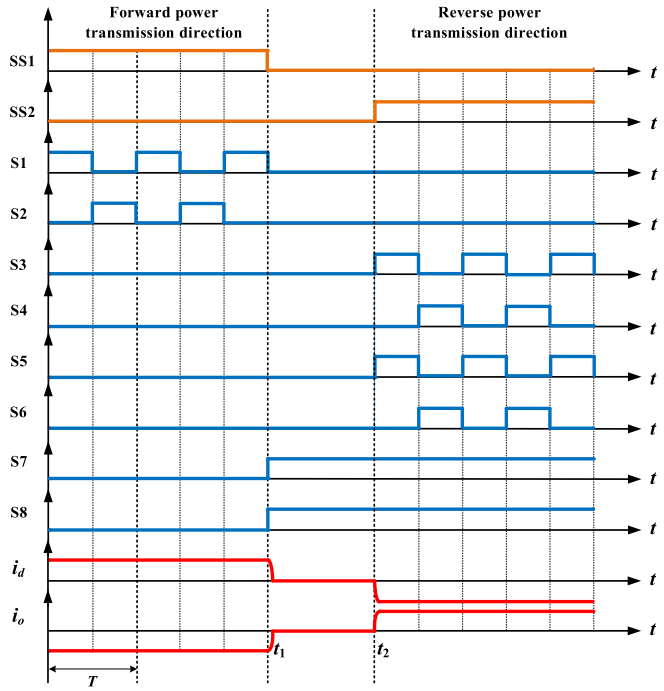

Fig. 7. Switching pulses with all switches during both power directions.

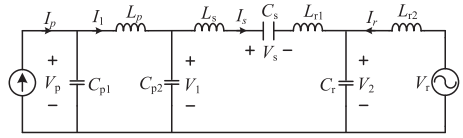

Fig. 8. Simplified equivalent ac-side circuit model of the proposed BCPT system.

"OFF." Besides, the resistance branch of the load R_{or} is "ON," while the power source branch V_o is "OFF."

When $t=t_1$, the branch of *SS*1 switched the power source to load. The push–pull converter stops working, the switches *S*1, *S*2 are turned OFF, and *S*7, *S*8 are turned ON. In this time, the current and voltage directions change process of the system circuit elements is complex, supposing that the switches of the full-bridge converter are switched ON suddenly at this time, it may lead to instability in the switching process, short circuit, current and voltage impact, and other safety problems. Especially at the moment of switching from reverse to forward transmission, the ZVS switching state of the system may be destroyed. Therefore, the system is reset to zero before switching the power flow direction; that is, when $t_1<t<t_2$, the voltage and current in the system circuit are reduced to zero.

When $t=t_2$, the converter of the full bridge changes from rectifier to the inverter, the power source branch V_o with the full-bridge converter is "ON," and the resistance branch R_{or} is "OFF." After that, the system operates in the reverse power transmission operation.

D. Characteristic Analysis of System Topology

The equivalent ac circuit model of the proposed push–pull full-bridge hybrid resonant topology BCPT system is shown in Fig. 8, where the input and output of the converters are modeled

as a current source and voltage source during the forward and reverse power transmissions, respectively.

According to KVL's law, the relationship between the currents and voltages can be derived as follows:

$$\begin{cases} \dot{V}_1 = \dot{V}_p - j\omega L_p \dot{I}_1 \\ \dot{V}_2 = \dot{V}_1 - Z \cdot \dot{I}_s \\ \dot{V}_r = \dot{V}_2 + j\omega L_{r2} \dot{I}_r \\ \dot{I}_s = \dot{I}_1 - j\omega C_{p2} \dot{V}_1 \\ \dot{I}_r = -\dot{I}_s + j\omega C_r \dot{V}_2 \\ \dot{I}_p = \dot{I}_1 + jwC_{p1} \dot{V}_p \end{cases} \tag{1}$$

where

$$Z = j\omega L_{r1} + j\omega L_s + \frac{1}{j\omega C_s}. \tag{2}$$

Power transmission, the current across the inductor L_{r2} can be derived as $\dot{I}_r = -\dot{V}_r / R_{er}$, where R_{er} is the equivalent load resistance at the input of the full-bridge converter circuit and can be calculated as

$$R_{er} = \frac{8}{\pi^2} R_r. \tag{3}$$

The output voltage of the full-bridge converter (reversible rectifier) during forward power transmission direction can be obtained as

$$\dot{V}_r = \dot{V}_p / [(1 - \omega^2 L_p C_{p2})(j\omega L_{r2} + R_{er}) / R_{er} + ((1 - \omega^2 L_p C_{p2}) Z + j\omega L_p)(j\omega C_r + (1 - \omega^2 L_{r2} C_r) R_{er})]. \tag{4}$$

Besides, during reverse power transmission direction, using power balance at the input and output of the current-fed push–pull converter circuit, the voltage and current expressions are given as

$$\begin{cases} I_p = \frac{\sqrt{2}}{\pi} I_d \\ V_p = \frac{\pi}{\sqrt{2}} V_d. \end{cases} \tag{5}$$

R_{ep} is the equivalent load resistance at the input of the push–pull converter circuit and is calculated as

$$R_{ep} = \frac{\pi^2}{2} R_p. \tag{6}$$

The input ac voltage of the push–pull converter circuit can be expressed as

$$\dot{V}_p = -\dot{I}_p R_{ep}. \tag{7}$$

Thus, the output voltage of the push–pull converter (reversible rectifier) during reverse power transmission can be obtained as

$$\dot{V}_p = \dot{V}_r \Bigg/ \Bigg[(1 - \omega^2 L_{r2} C_r) \left((1 + j\omega C_{p2} Z) - (j\omega L_p + (1 - \omega^2 L_p C_{p2}) Z) \left(\frac{1}{R_{ep}} - j\omega C_{p1} R_{ep} \right) \right) + j\omega L_{r2} \left((1 - \omega^2 L_p C_{p2}) \left(\frac{1}{R_{ep}} - j\omega C_{p1} R_{ep} \right) + j\omega C_{p2} \right) \Bigg]. \tag{8}$$

Assuming the compensation network is fully resonant, the resonant frequency should satisfy

$$\omega^2 L_r C_r = 1, \quad \omega^2 L_p C_p = 1, \quad \omega^2 L_s C_s = 1 \tag{9}$$

where

$$C_p = C_{p1} = C_{p2}, \quad L_r = L_{r1} = L_{r2}. \tag{10}$$

Therefore, the voltage gain with the proposed BCPT system can be obtained as

$$G_{\mathrm{v\_}f} = \frac{1}{G_{\mathrm{v\_}r}} = \frac{\dot{V}_r}{\dot{V}_p} = -\frac{C_p}{C_r} \tag{11}$$

where G_{v_f} and G_{v-r} refer to the voltage gain during the forward and reverse power transmissions, respectively.

From the above analysis, the conclusion is drawn that the voltage gain is related to the ratio of capacitors C_p and C_r, and the output voltage is almost load independent during both power transmission directions.

III. Power Flow Control in BCPT System

In order to realize the power flow control of the proposed BCPT system, multiple ZVS soft-switching operating points switching and the phase-shifting regulation methods are adopted without adding additional circuits during forward and reverse power transmission directions, respectively.

A. Switching ZVS Soft-Switching Operating Points Power Regulation During Forward Power Transmission

During forward power transmission direction, switching ZVS soft-switching operating points power regulation technique is utilized to achieve the required power [21]. The proposed system can be linearized into two operating modes when the push–pull converter switches *S*1 and *S*2 conduct complimentary, while *S*7 and *S*8 kept OFF.

When *S*1 is ON and *S*2 is OFF, a positive output voltage appears at the push–pull converter, and the steady-state duration is $t_1 = T/2$.

When S1 is OFF and S2 is ON, a negative output voltage appears at the push–pull converter, and the steady-state duration is $t_2 = T/2$.

Taking the voltage of capacitances and the current of inductors in the system as the state variables, $x = [i_d \ i_p \ v_p \ i_1 \ v_1 \ i_s \ v_s \ v_2 \ i_r]^T$ and $u = [V_d]$ are the state vector and the input vector of the system, respectively, then the differential equation can be expressed by the state-space description equation as follows:

$$\begin{cases} \dot{x} = A_1 x + B_1 u \ \text{mode1} \\ \dot{x} = A_2 x + B_2 u \ \text{mode2} \end{cases} \tag{12}$$

where A_1, A_2 are the system coefficient matrices, and B_1, B_2 are the system input matrices.

Under the two linear operating modes, the system time mapping function is

$$x(t) = \Phi_i(t) x_0 + (\Phi_i(t) - I) A_i^{-1} B_i u_i \ (i = 1, 2) \tag{13}$$

where $\Phi_i(t) = e^{Ai(t)}$ is the system state transition matrix, and $x_0 = x(0)$ is the initial state of the mode.

The operating duration of each linear mode is t_i, and the system steady-state operation period is $T = t_1 + t_2$.

Then, the state mapping function of each mode is obtained as follows:

$$f_{i,t_i}(x) = \Phi_i(t_i)\, x + (\Phi_i(t_i) - I)\, {A_i}^{-1} B_i u_i \ (i = 1, 2). \tag{14}$$

Assuming that x_n and x_{n+1} are the initial and the end states of the cycle, respectively, the stroboscopic mapping model of the nth working cycle is as follows:

$$\begin{aligned} x_{n+1} &= f_{2,t_2} \circ f_{1,t_1}(x_n) \\ &= \Phi_2\left(\frac{T}{2}\right)\left(\Phi_1\left(\frac{T}{2}\right) x_n + \left(\Phi_1\left(\frac{T}{2}\right) - I\right) {A_1}^{-1} B_1 E_{\mathrm{dc}}\right) \\ &\quad + \left(\Phi_2\left(\frac{T}{2}\right) - I\right) {A_2}^{-1} B_2 E_{\mathrm{dc}} \end{aligned} \tag{15}$$

where $\circ$ represents a composite mapping operator and can be defined as $f \circ g(t) = f(g(t))$.

The system state vector repeats periodically when the system reaches a steady state

$$x_{n+1} = x_n. \tag{16}$$

The system periodic fixed-point x^* is obtained as

$$\begin{aligned} x^* &= f_{2,\xi_2} \circ f_{1,\xi_1}(x^*) \\ &= \left(I - \Phi_2\left(\frac{T}{2}\right)\Phi_1\left(\frac{T}{2}\right)\right)^{-1} \\ &\quad \times \begin{pmatrix} \Phi_2\left(\frac{T}{2}\right)\left(\Phi_1\left(\frac{T}{2}\right) - I\right) {A_1}^{-1} B_1 E_{\mathrm{dc}} \\ + \left(\Phi_2\left(\frac{T}{2}\right) - I\right) {A_2}^{-1} B_2 E_{\mathrm{dc}} \end{pmatrix}. \end{aligned} \tag{17}$$

The periodic fixed-point x^* of the system can be regarded as a function of the period T when T is regarded as a variable. The component v_p in the fixed-point x^* is used to analyze the system fixed-point function with the ZVS soft-switching operation points, and v_p can be obtained as follows:

$$\begin{aligned} v_p(t) &= Y\left(I - \Phi_2\left(\frac{t}{2}\right)\Phi_1\left(\frac{t}{2}\right)\right)^{-1} \\ &\quad \times \begin{pmatrix} \Phi_2\left(\frac{t}{2}\right)\left(\Phi_1\left(\frac{t}{2}\right) - I\right) {A_1}^{-1} B_1 u \\ + \left(\Phi_2\left(\frac{t}{2}\right) - I\right) {A_2}^{-1} B_2 u \end{pmatrix} \end{aligned} \tag{18}$$

where

$$\Phi_i(t) = e^{A_i t} \quad i = 1, 2 \tag{19}$$

$$Y = \begin{bmatrix} 0\,0\,1\,0\,0\,0\,0\,0\,0 \end{bmatrix}. \tag{20}$$

Matrix Y represents the projective matrix used to extract the output voltage component of the push–pull converter from the state variable x.

To achieve ZVS soft-switching operation, v_p should be satisfied as follows:

$$v_p(t) = 0. \tag{21}$$

Therefore, from (21), we can get the ZVS soft-switching operation points that are used to regulate the power.

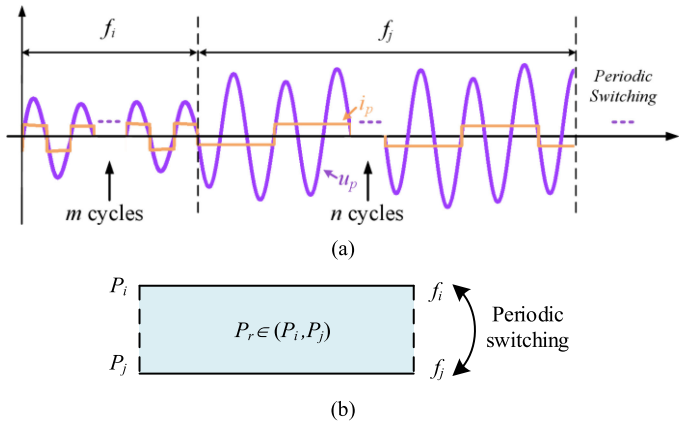

Fig. 9. Diagram of power regulation by switching multiple ZVS soft-switching operating points. (a) Shifting among multiple soft-switching operating points. (b) Approximate power transfer capability between the two ZVS soft-switching operating points.

Fig. 9(a) shows the schematic diagram switches shifting between two ZVS soft-switching operating points. The system operates m cycles at frequency f_i and n cycles at frequency f_j. The purple sine curve shows the waveform of the push–pull converter output voltage v_p, and the orange pulse shows the output current i_p. Fig. 9(b) shows the system power P_i when the soft-switching operating frequency is f_i, whereas P_j is corresponding to f_j. Power can be regulated to achieve the required power P_r by switching back and forth between the two ZVS soft-switching operating points.

B. Phase-Shifted Power Regulation During Reverse Power Transmission

During reverse power transmission direction, the full-bridge converter acts as an inverter and converts voltage from dc to high-frequency ac voltage v_r. The push–pull converter will act as a rectifier and converts high-frequency ac current i_p to dc current. The phase-shift control method is utilized to regulate the output voltage of the full-bridge converter, and the power injected into the push–pull converter can be regulated effectively by modulating the phase-shift angle between switches of the full-bridge converter.

The driving signals of the switches and the output voltage of the full-bridge converter are provided, as shown in Fig. 10. A phase-shifted pulse is provided to switches S3 and S5, and diagonal switches S4 and S6 are switched ON simultaneously with a duty cycle of 50%. By modulating the phase-shift angle θ, the output voltage of the full bridge can be changed to regulate the output power.

The output voltage of the full-bridge converter is as follows:

$$V_r = \frac{2\sqrt{2}}{\pi} V_o \cos\left(\frac{\theta}{2}\right) \ (0 \le \theta < \pi). \tag{22}$$

Using (11) and (22), it is clear that the output power of the reverse power transmission direction is derived as

$$P_p = V_p I_p \mathrm{Re}[e^{j(\varphi_{v_p} - \varphi_{i_p})}] = \frac{16 L_p^2 V_o^2 \cos^2\left(\frac{\theta}{2}\right)}{\pi^4 L_r^2 R_p}. \tag{23}$$

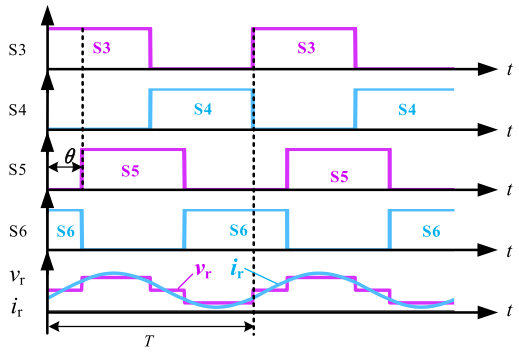

Fig. 10. Switching pulses and the voltage generated with the full-bridge converter.

TABLE II
PARAMETERS OF THE PROPOSED BCPT SYSTEM

Parameter	Value	Parameter	Value
V_d(V)	35	V_o(V)	130
L_{d1}/L_{d2} (mH)	480	R_{Ld1} /R_{Ld2}(mΩ)	400
L_p (μH)	5	C_{p1}/C_{p2} (nF)	20
C_{s1} (pF)	1200	C_{s2} (pF)	858
L_s (μH)	200	L_{r1}/L_{r2} (μH)	27
C_r (nF)	3.75	C_o (μF)	47
R_{op} (Ω)	25	R_{or} (Ω)	150

IV. System Performance Analysis

To give a further comprehension of the proposed asymmetrical power conversion mode, system performance analysis on the output voltage and power regulation is implemented as follows.

A. Parameter Design of the Proposed BCPT System

In Section II-D, the output voltage is almost load independent during both directions. The operating frequency of the proposed BCPT system is set to $f = 500$ kHz. In order to minimize the harmonic distortion rate of the proposed high-order system, the quality factor Q_π of π structure should be larger and Q_T should be smaller. However, too large Q_π and too small Q_T will cause the input impedance angle of the resonant network to be sensitive to the change of frequency. As a compromise, the upper limit of Q_π is 3 and the lower limit of Q_T is 0.5 [16]. Therefore, the range of two capacitance ratios C_p/C_r is obtained as (0.167, 6). From (9), in order to reduce the resonance inductance in the high-frequency environment, the value of C_p is 5 nF and C_r is 3.75 nF. In addition, due to the voltage pumping characteristics of the push–pull converter circuit, given that the system input voltage of forward power transmission is 35 V, the full-bridge converter load $R_r = 150$ Ω to obtain the output power is approximately 100 W. Besides, the load R_p of the push–pull converter is 25 Ω. Therefore, the appropriate parameters of the BCPT system are designed and listed in Table II.

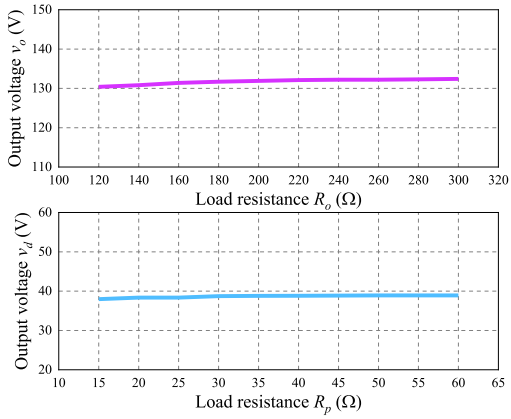

Fig. 11. Output voltage varies with loads in the bidirectional power transmission direction.

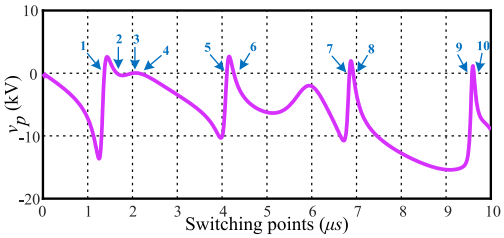

Fig. 12. Push–pull converter output voltages v_p under different ZVS soft-switching operating periods.

B. Output Characteristic Analysis of the Proposed System

From the parameter values in Table II, the curve of output voltage with different load resistances in bidirectional power transmission direction is obtained, as shown in Fig. 11. The purple and blue lines represent the output voltage with the varying load during forward and reverse power transmissions, respectively. The voltage fluctuation rate is within 2% in the range of load from 100 to 300 Ω during forward power transmission. The voltage fluctuation rate is within 4% in the range of load from 15 to 60 Ω during reverse power transmission. Therefore, approximate voltage output constant characteristics in bidirectional power transmission can be achieved under the framework of the π-T resonant and asymmetrical power converters.

C. Bidirectional Power Regulation Analysis of the Proposed BCPT System

1) Forward Power Regulation Method by Switching ZVS Soft-Switching Frequency: The proposed system adopts the ZVS soft-switching operating point switching for power regulating during forward power transmission. According to the parameters given in Table II, the periodic fixed-point function formula (18) of the push–pull converter output voltage is shown in Fig. 12.

By considering the boundary condition (21), all zero-crossing points of the push–pull converter output voltage represent the ZVS switching periods. Fig. 10 shows the eight ZVS soft-switching periods in the time of (0, 10 μs), corresponding to the ZVS switching frequencies existing in the proposed system,

TABLE III
ZVS SOFT-SWITCHING OPERATING PERIODS AND FREQUENCIES OF THE PROPOSED BCPT SYSTEM DURING FORWARD POWER TRANSMISSION

ZVS points	1	2	3	4	5	6	7	8
ZVS periods (μs)	1.38	1.66	2.01	2.13	4.11	4.27	6.85	6.93
f_{zvs} (kHz)	725	602	498	469	243	234	146	144

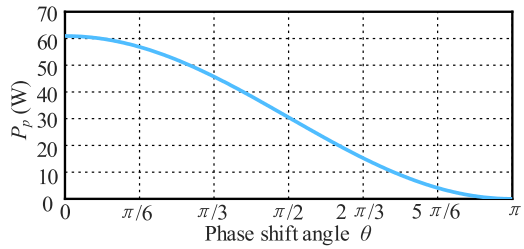

Fig. 13. System output power varies with phase-shift angle during reverse power transmission direction.

as given in Table III. Each ZVS soft-switching frequency corresponds to the different output powers, respectively, which can obtain the expected power by switching two frequencies.

2) Reverse Power Regulation Method by Phase-Shifted Control Strategy: From (23), the output power is regulated by the phase shift during reverse power transmission, as shown in Fig. 13. It shows that the power decreases with the increase of the phase-shift angle θ during reverse power transmission direction.

V. EXPERIMENTAL RESULTS

In order to validate the feasibility of the proposed bidirectional power flow transmission, a BCPT system prototype is implemented, as shown in Fig. 14(a). Considering the short-distance application for the charging of electronic devices, the disc capacitive coupler is shown in Fig. 14(b).

The copper foil with a thickness of 0.15 mm is used as the coupling plates $P1$, $P2$, $P3$, and $P4$; the size of one pair plate is 85 mm∗85 mm, which is placed on the received side as the receiver, and the other pair uses a ring with the radius from 95 to 130 mm, which is plated on the other side as the transmitter. Litz-wire winding magnetic core constitutes the compensation inductors L_s, L_p and L_{r2} are made of Litz-wire wound on polyvinyl chloride tubes, and the other capacitors use the chip capacitor. GS66504B is used as GaN gate driver, and the controller is equipped with a complex programmable logic device (CPLD, EPM240T100C5), which is used to generate the drive signals of the converters. Power source and load are switched by relay-operated switches on both sides.

A. Forward Power Transmission Tests

Fig. 15 shows the experimental results with the output power of 112 W during forward power transmission, and the ZVS soft-switching frequency of the push–pull converter is 491.7 kHz. When the dc input voltage V_d is 35 V, the output voltage V_o is 130 V. Fig. 15(a) shows the ZVS turn-OFF of the forward-side converter switches operating at the ZVS soft-switching

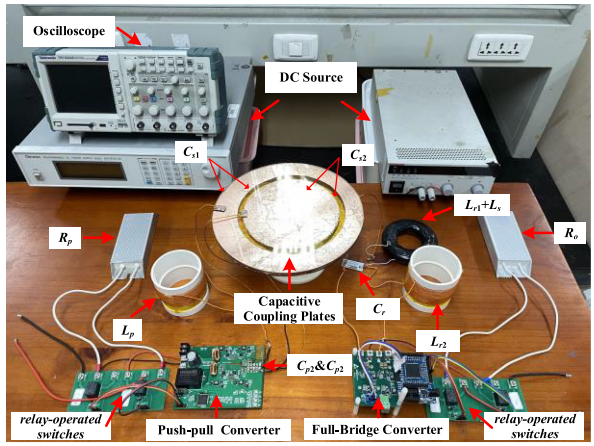

Fig. 14. Experimental setup. (a) Prototype of the proposed BCPT system. (b) Structure and size of the coupling plates.

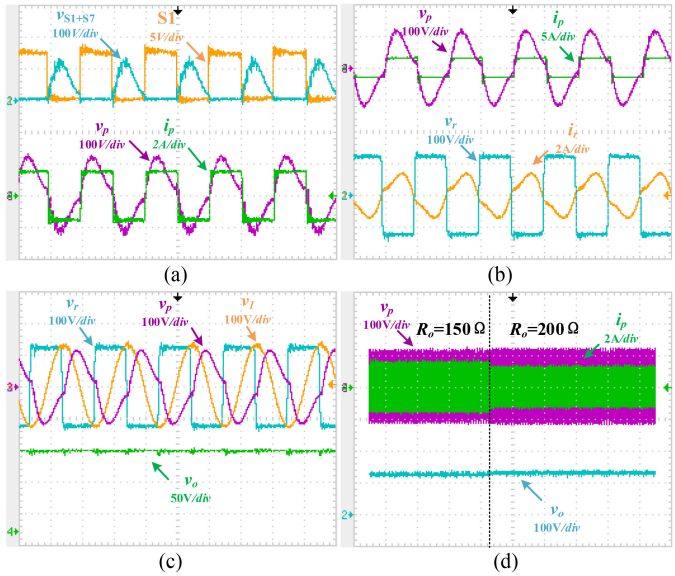

Fig. 15. Experimental results of forward power transmission at ZVS soft-switching operation frequency $f_{s1} = 491.7$ kHz, $V_d = 35$ V, $P_o = 112$ W, and $V_o = 130$ V. (a) Driving signal $S1$, the voltages of $S1$ and $S7$, and the resonant voltage and current of the push–pull converter. (b) Voltages and currents at the push–pull and full-bridge converters. (c) Input and output voltages with the topology structure π and T, and the output voltage V_o of load. (d) Resonant voltage and current of the push–pull converter and V_o.

operating point. The current-fed push–pull converter voltage and current profiles are in the same phase. Fig. 15(b) shows the experimental voltages and currents' waveforms for both side converters during forward power transmission operations. Fig. 15(c) shows the profiles of the input and output voltages with the topology structure $\pi-$T and the output voltage of

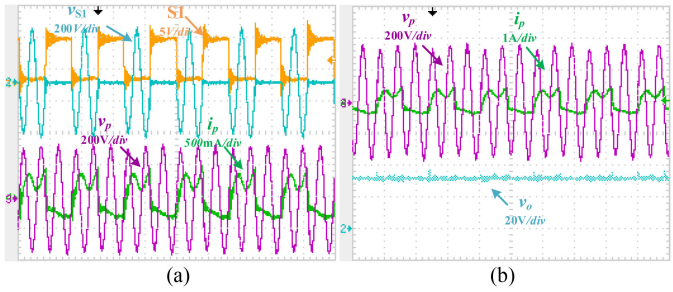

Fig. 16. Experimental results of forward power transmission at operating frequency $f_{s2} = 242.6$ kHz, $V_d = 35$ V, $P_o = 6.4$ W, and $V_o = 31$ V. (a) Driving signal $S1$, the voltages of $S1$ and $S7$, and the voltage and current of the push–pull converter. (b) Voltage and current at the push–pull converter and the output voltage of load R_{or}.

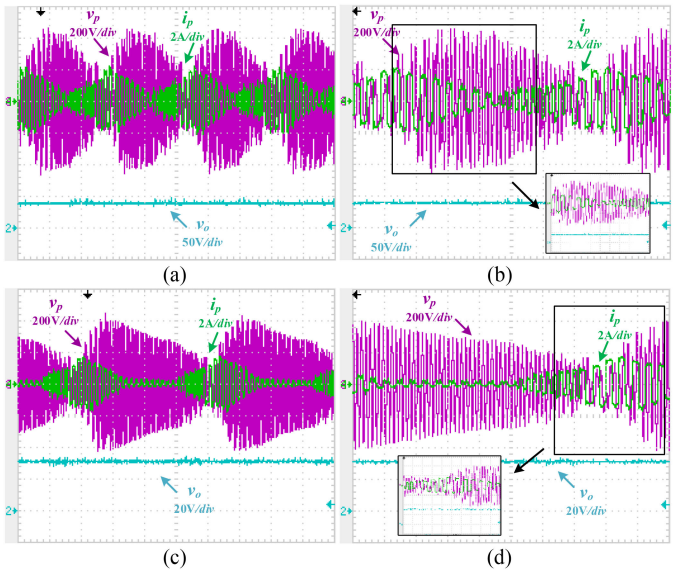

Fig. 17. Experimental results with power regulation of two ZVS soft-switching operating points dynamics switching with frequencies $f_{s1} = 491.7$ kHz and $f_{s2} = 242.6$ kHz. (a) Operating at f_{s1} with 10 cycles and operate at f_{s2} with 10 cycles, $V_d = 20$ V, $P_o = 10.7$ W, and $V_o = 40$ V. (b) Enlarged view of figure (a). (c) Operating at f_{s1} with 10 cycles and operating at f_{s2} with 20 cycles, $V_d = 20$ V, $P_o = 6.8$ W, and $V_o = 32$ V. (d) Enlarged view of figure.

load R_{or}. Fig. 15(d) shows the dynamic response when the load R_{or} is switched from 150 to 200 Ω, it validates the characteristic of the proposed topology with constant voltage characteristics during forward power transmission direction.

Fig. 16 shows that the system operated in another ZVS soft-switching frequency of 242.6 kHz, and V_d is 35 V; the system output power is 6.4 W. Fig. 16(a) shows the ZVS turn-OFF of the forward-side converter switches operating at soft-switching frequency 242.6 kHz. Besides, forward-side converter voltage and current profiles are in the same phase. Fig. 16(b) shows the experimental voltage and current waveforms for the push–pull converter, and the output voltage V_o of the load R_{or} is 31 V during forward power transmission operations.

Fig. 17 validates the power regulation of switching between two ZVS operation frequencies in dynamics power regulation

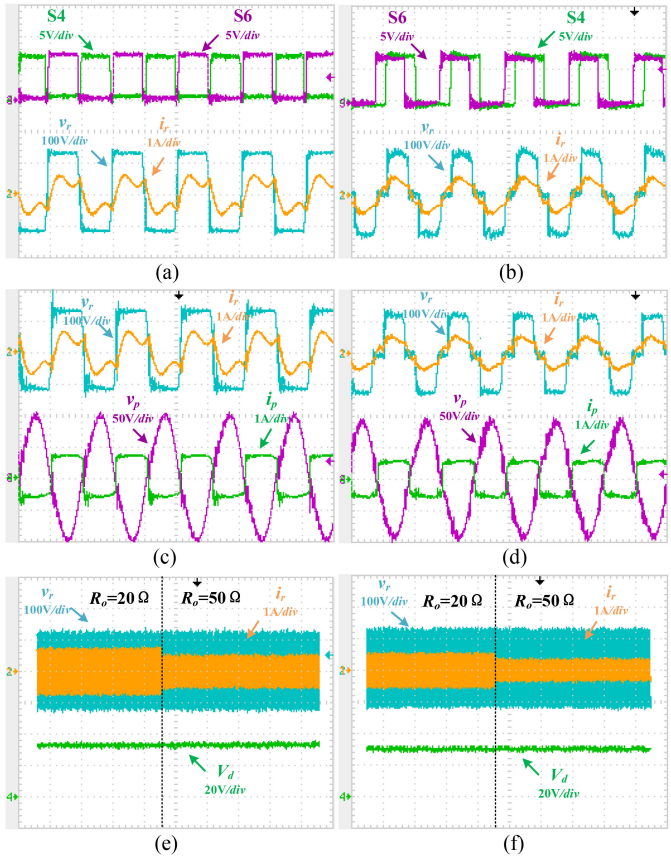

Fig. 18. Experimental results of reverse power transmission operation: $V_o = 130$ V, $V_d = 35$ V, $P_d = 49$ W at phase-shift angle 0°; and $V_d = 30$ V, $P_d = 36$ W at phase-shift angle 60°. (a) Driving signal and voltage of $S3$, and output voltage and current of the full-bridge converter. (b) Driving signal $S3$ and $S5$, and the output voltage and current of the full-bridge converter. (c) Voltages and currents of the full-bridge converter output and the push–pull converter input at phase-shift angle 0°. (d) Voltages and currents of the full-bridge and the push–pull converter at phase-shift angle 60°. (e) Voltage and current of the full-bridge converter and output voltage of load R_{op} at phase-shift angle 0°. (f) Voltage and current of the full-bridge converter and output voltage of load R_{op} at phase-shift angle 60°.

during forward power transmission operation, which shows the envelope fluctuation of resonant voltage and current. When the system dc input voltage $V_d = 20$ V, Fig. 17(a) and (b) shows the system operating at frequency f_{s1} with 10 cycles and f_{s2} with 10 cycles, and continuously switching the two frequencies, the system output power is 10.7 W. Fig. 17(c) and (d) shows the system operating on frequency f_{s1} with 10 cycles and f_{s2} with 20 cycles, and after continuously switching the two frequencies, the output power is 6.8 W.

B. Reverse Power Transmission Tests

Fig. 18 shows the system output power experimental results of 49 and 36 W at phase-shift angles 0° and 60°, respectively, during reverse power transmission operation.

When the dc input voltage V_o is 130 V, Fig. 18(a) and (b) presents the driving signal $S3$, $S5$ and the output resonant voltage and current waveforms of the full-bridge converter when the phase-shift angle is 0° and 60°, respectively. Fig. 18(c) and 18(d)

TABLE IV
COMPARISON OF CRITICAL PERFORMANCE CHARACTERISTICS WITH SYMMETRICAL CPT SYSTEMS

	Topology	Power	Switches	Inductors	Voltage Gain	Efficiency	Transient Response	Power Source Type	Bidirectional Power Regulation Function	Asymmetrical resonant topology	Bidirectional power transmission
Paper [19]	Dual LC	150W	4	2	1.08	Higher than 70%	Not mentioned	Voltage source	Not	symmetric	Unidirectional
Paper [17]	Dual LCL	1.87kW	4	4	1	85.87%	Not mentioned	Voltage source	Not	symmetric	Unidirectional
Paper [18]	Dual LCLC	2.1kW	4	4	1.06	90.7%	Not mentioned	Voltage source	Not	symmetric	Unidirectional
Paper [20]	Dual LCLC	100W	8	4	0.8	80.15%	Not mentioned	Voltage source	Not	symmetric	Bidirectional
This paper	π-T	100W	8	5	3.7	Forward: 81.4% Reverse: 82%	Mentioned	Current and Voltage source	Yes	Asymmetric	Bidirectional

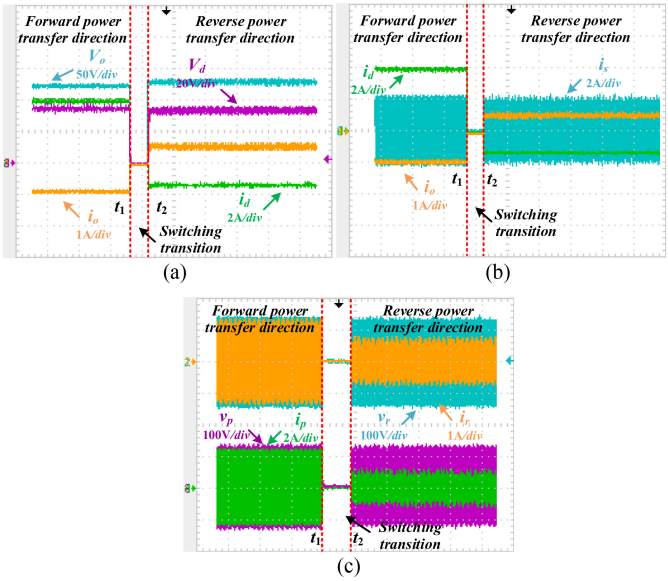

Fig. 19. Dynamic switching process of the system. (a) DC voltage V_d, V_o and dc i_d, i_o. (b) DC i_d, i_o and the current across the coupling plates i_s. (c) AC equivalent voltages and currents of the full-bridge and the push–pull converter.

shows the resonant voltages and currents with the full-bridge and the push–pull converters. From Fig. 18(e) and (f), system output voltage V_d is 35 V and 30 V at phase-shift angle 0° and 60°, respectively. Besides, the output voltage of load remains constant despite the changes with R_{op} from 20 to 50 Ω.

C. Dynamic Switching Process

The system dynamic switching process from forward to reverse power transmission is shown in Fig. 19. As shown in Fig. 19(a), when $t<t_1$, the system operates in the forward power transmission, the push–pull converter acts as the inverter, while the full-bridge converter is the rectifier, and the load resistance R_{or} receives energy. The dc input voltage V_d is 35 V, i_d is +4 A, the load output voltage V_o is 130 V, and i_o is −0.88 A; when $t=t_1$, the power source is switched to the load R_{op}, the push–pull converter stops working, $S1$, $S2$ are turned OFF, and $S7$, $S8$ are turned ON. At this time, V_d, i_d, V_o, and i_o are 0; when $t=t_2$, the load resistance R_{or} is switched to the power source branch V_o, the full-bridge converter operates as the inverter, and the push–pull converter operates as the rectifier. The dc input voltage V_o is 130 V, i_o is +0.5 A, and i_d is −1.5 A. Fig. 19(b) shows the dc currents i_d and i_o and the current i_s passing through the coupling plates. Fig. 19(c) shows the output voltages and currents of the push–pull and full-bridge converters, where v_p and i_p represent the ac equivalent voltage and current of the push–pull converter, and v_r and i_r represent the ac equivalent voltage and current of the full-bridge converter.

D. Comparison With Other Symmetrical CPT System

The comparison with other symmetrical CPT systems in terms of switches, inductors, gain, efficiency, transient response, and so on is given in Table IV. Compared with the symmetrical resonant topology CPT systems, as shown in [17]–[20], the proposed BCPT system adopted the asymmetric topology and realized bidirectional power flow regulation. Among them, Zhang *et al.* [17] and [18] proposed unidirectional CPT systems and reached an efficiency of more than 85% or even 90%, but the system transmission power is kilowatt power level. According to the analysis of the efficiency-power curves in [17] and [18], the system efficiency keeps increasing with the increase of the output power. Besides, Yang *et al.* [20] utilize the same symmetrical *LCLC*-compensated topology as the article presented in [18], and the system efficiency is 80.15% when the power is 100 W. Moreover, under the same hundred-watt power level, the symmetrical system efficiency in [19] is about 70%. Besides, Yang *et al.* [20] proposed a bidirectional symmetrical CPT system with dual *LCLC* topology and the efficiency is about 80%. However, they did not mention the power flow regulation method and dynamic switching transient response. The proposed BCPT system adopts an asymmetric hybrid (π–T) resonant topology, mixing two different power source types (current-fed push–pull and voltage-fed full bridge) together with two different power regulation modes. Besides, the proposed system achieves a high forward voltage gain of 3.7, and this system achieves 100 W output power during forward power transmission. The efficiency from the source to the load, including the power electronics circuit, reaches 81.4%. During reverse power transmission, as

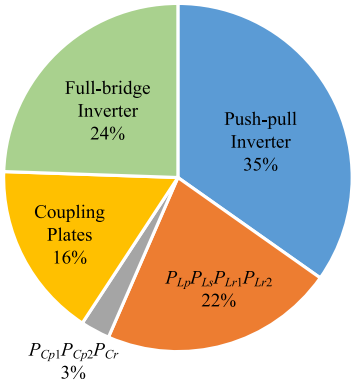

Fig. 20. Power loss distribution within the circuit components.

the input dc voltage reaches 130 V, the system achieves 50 W output power. The efficiency reaches 82%.

VI. Discussion

The estimated power loss distribution among the system circuit components is analyzed, as shown in Fig. 20. The power loss of the proposed system is mainly distributed in the converters, compensation inductors, capacitors, and coupling plates (the calculation method of power loss distribution refers to the article presented in [22]). The push–pull converter dissipates approximately 35% of the power loss, and the full-bridge converter dissipates about 24% of the power loss, mainly because the operating frequency of the IPT system is usually 85 kHz, while that of the CPT system is hundreds of kilohertz to megahertz; the loss caused by the conduction, turn-OFF, and switching of the switches is higher than those of IPT system. The proportion of the converter power loss is high in the low-power transmission system, and it will be greatly improved after the power is increased.

VII. Conclusion

This article proposed an asymmetric push–pull full-bridge hybrid (π–T) resonant topology BCPT system, and the main contribution of the proposed method can be concluded as follows.

1) The asymmetrical topology can unlock more current-fed resonant topologies for the BCPT system to make it adaptive to present CPT applications. Furthermore, the mixing asymmetrical topology is suitable for the equipment with two different input or output characteristics' requirements.
2) The asymmetrical topology can provide the BCPT system with a load tolerance region that can overcome sensitivity problems brought by load variation.
3) Multifrequencies bidirectional power transmission realization. By using multiple ZVS soft-switching operating points, the system can operate at different frequencies in the forward power transmission. It provides a more flexible regulation method for bidirectional power transmission with nonequal power rating devices.

Acknowledgment

The authors would like to thank the support of the China National Center for International Research on Wireless Power Transfer Technology.

References

[1] D. J. Graham, J. A. Neasham, and B. S. Sharif, "Investigation of methods for data communication and power delivery through metals," *IEEE Trans. Ind. Electron.*, vol. 58, no. 10, pp. 4972–4980, Oct. 2011.
[2] M. N. Kheraluwala, R. W. Gascoigne, D. M. Divan, and E. D. Baumann, "Performance characterization of a high-power dual active bridge dc-to-dc converter," *IEEE Trans. Ind. Appl.*, vol. 28, no. 6, pp. 1294–1301, Nov./Dec. 1992.
[3] Y. Jang and M. M. Jovanovic, "A contactless electrical energy transmission system for portable-telephone battery chargers," *IEEE Trans. Ind. Electron.*, vol. 50, no. 3, pp. 520–527, Jun. 2003.
[4] J. Wu, X. Dai, R. Gao, and J. Jiang, "A coupling mechanism with multidegree freedom for bidirectional multistage WPT system," *IEEE Trans. Power Electron.*, vol. 36, no. 2, pp. 1376–1387, Feb. 2021.
[5] U. K. Madawala and D. J. Thrimawithana, "A bidirectional inductive power interface for electric vehicles in V2G systems," *IEEE Trans. Ind. Electron.*, vol. 58, no. 10, pp. 4789–4796, Oct. 2011.
[6] A. A. S. Mohamed, A. Berzoy, and O. A. Mohammed, "Experimental validation of comprehensive steady-state analytical model of bidirectional WPT system in EVs applications," *IEEE Trans. Veh. Technol.*, vol. 66, no. 7, pp. 5584–5594, Jul. 2017.
[7] D. J. Thrimawithana and U. K. Madawala, "A generalized steady-state model for bidirectional IPT systems," *IEEE Trans. Power Electron.*, vol. 28, no. 10, pp. 4681–4689, Oct. 2013.
[8] C. Liu, A. P. Hu, and N.-K. C. Nair, "Modelling and analysis of a capacitively coupled contactless power transfer system," *IET Power Electron.*, vol. 4, no. 7, pp. 808–815, Sep. 2011.
[9] X. Dai, X. Li, Y. Li, and A. P. Hu, "Maximum efficiency tracking for wireless power transfer systems with dynamic coupling coefficient estimation," *IEEE Trans. Power Electron.*, vol. 33, no. 6, pp. 5005–5015, Jun. 2018.
[10] L. Huang, A. P. Hu, A. Swain, S. Kim, and Y. Ren, "An overview of capacitively coupled power transfer—A new contactless power transfer solution," in *Proc. IEEE 8th Conf. Ind. Electron. Appl.*, 2013, pp. 461–465.
[11] Y.-G. Su, W. Zhou, A. P. Hu, C.-S. Tang, S.-Y. Xie, and Y. Sun, "Full-duplex communication on the shared channel of a capacitively coupled power transfer system," *IEEE Trans. Power Electron.*, vol. 32, no. 4, pp. 3229–3239, Apr. 2017.
[12] D. C. Ludois, J. K. Reed, and K. Hanson, "Capacitive power transfer for rotor field current in synchronous machines," *IEEE Trans. Power Electron.*, vol. 27, no. 11, pp. 4638–4645, Nov. 2012.
[13] A. P. Hu, C. Liu, and H. L. Li, "A novel contactless battery charging system for soccer playing robot," in *Proc. 15th Int. Conf. Mechatronics Mach. Vis. Pract.*, 2008, pp. 646–650.
[14] R. Sedehi *et al.*, "A wireless power method for deeply implanted biomedical devices via capacitively coupled conductive power transfer," *IEEE Trans. Power Electron.*, vol. 36, no. 2, pp. 1870–1882, Feb. 2021, doi: 10.1109/TPEL.2020.3009048.
[15] J.-Q. Zhu *et al.*, "A novel capacitive coupler array with free-positioning feature for mobile tablet applications," *IEEE Trans. Power Electron.*, vol. 34, no. 7, pp. 6014–6019, Jul. 2019, doi: 10.1109/TPEL.2018.2888623.
[16] Y.-G. Su, S.-Y. Xie, A. P. Hu, C.-S. Tang, W. Zhou, and L. Huang, "A capacitive power transfer system with a mixed-resonant topology for constant-current multiple-pickup applications," *IEEE Trans. Power Electron.*, vol. 32, no. 11, pp. 8778–8786, Nov. 2017.
[17] H. Zhang, F. Lu, H. Hofmann, W. Liu, and C. C. Mi, "A four-plate compact capacitive coupler design and LCL-compensated topology for capacitive power transfer in electric vehicle charging application," *IEEE Trans. Power Electron.*, vol. 31, no. 12, pp. 8541–8551, Dec. 2016.
[18] F. Lu, H. Zhang, H. Hofmann, and C. Mi, "A double-sided LCLC-compensated capacitive power transfer system for electric vehicle charging," *IEEE Trans. Power Electron.*, vol. 30, no. 11, pp. 6011–6014, Nov. 2015.
[19] F. Lu, H. Zhang, H. Hofmann, and C. C. Mi, "A double-sided LC-compensation circuit for loosely coupled capacitive power transfer," *IEEE Trans. Power Electron.*, vol. 33, no. 2, pp. 1633–1643, Feb. 2018.

[20] L. Yang, M. Ju, and B. Zhang, "Bidirectional undersea capacitive wireless power transfer system," *IEEE Access*, vol. 7, pp. 121046–121054, 2019.
[21] C. S. Tang, Y. Sun, Y. G. Su, S. K. Nguang, and A. P. Hu, "Determining multiple steady-state ZCS operating points of a switch-mode contactless power transfer system," *IEEE Trans. Power Electron.*, vol. 24, no. 2, pp. 416–425, Feb. 2009.
[22] F. Lu, H. Zhang, H. Hofmann, and C. Mi, "A high efficiency 3.3 kw loosely-coupled wireless power transfer system without magnetic material," in *Proc. IEEE Energy Convers. Congr. Expo.*, 2015, pp. 2282–2286.

Xin Dai (Member, IEEE) received the B.S. degree in industrial automation from Yuzhou University, Chongqing, China, in 2000, and the Ph.D. degree in control theory and control engineering from the School of Automation, Chongqing University, Chongqing, China, in 2006.

In 2012, he was a Visiting Scholar with The University of Auckland, Auckland, New Zealand. He is currently a Professor with the School of Automation, Chongqing University. His research interests include inductive power transfer technology and nonlinear dynamic behavior analysis of power electronics.

Min Sun received the B.E. degree in automation from the College of Artificial Intelligence, Chongqing Technology and Business University, Chongqing, China, in 2017. She is currently working toward the Ph.D. degree in control theory and control engineering with Chongqing University, Chongqing, China.

Her current research interests include the bidirectional wireless power transfer and power electronics.

Pengqi Deng received the B.E. degree in automation in 2015 from the College of Automation, Chongqing University, Chongqing, China, where he is currently working toward the Ph.D. degree in control theory and control engineering.

His research interest includes modeling and control optimization of the wireless power transfer.

Rui Wang received the B.E. degree in automation in 2017 from the College of Automation, Chongqing University, Chongqing, China, where he is currently working toward the Ph.D. degree in control theory and control engineering.

His current research interests include control of wireless power transfer system and ultrasonic testing system.

Yugang Su (Member, IEEE) received the B.E. and M.E. degrees in industry automation and the Ph.D. degree in control theory and control engineering from Chongqing University, Chongqing, China, in 1985, 1993, and 2004, respectively.

From 2008 to 2009, he was a Visiting Scholar with the University of Queensland, Brisbane, QLD, Australia. He is currently a Professor with the College of Automation, Chongqing University. His research interests include power electronics, control theory and applications, and wireless power transfer.